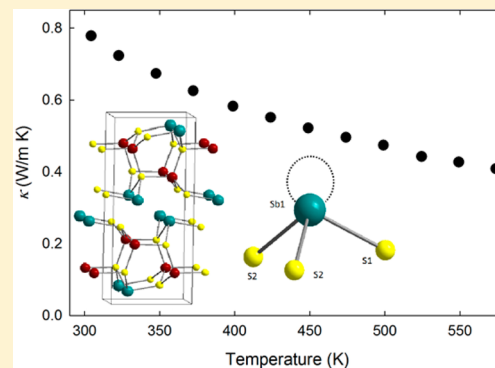


Synthesis, Structure, Te Alloying, and Physical Properties of CuSbS_2 Dean Hobbis,[†] Kaya Wei,[†] Hsin Wang,[‡] Joshua Martin,[§] and George S. Nolas^{*,†,§}[†]Department of Physics, University of South Florida, Tampa, Florida 33620, United States[‡]Materials Science and Technology Division, Oak Ridge National Laboratory, Oak Ridge, Tennessee 37831, United States[§]Material Measurement Laboratory, National Institute of Standards and Technology, Gaithersburg, Maryland 20899, United States

ABSTRACT: Materials with very low thermal conductivities continue to be of interest for a variety of applications. We synthesized CuSbS_2 employing a mechanical alloying technique in order to investigate its physical properties. The trigonal pyramid arrangement of the S atoms around the Sb atoms allows for lone-pair electron formation that results in very low thermal conductivity. In addition to thermal properties, the structural, electrical, and optical properties, as well as compositional stability measurements, are also discussed. $\text{CuSbS}_{1.8}\text{Te}_{0.2}$ was similarly synthesized and characterized in order to compare its structural and transport properties with that of CuSbS_2 , in addition to investigating the effect of Te alloying on these properties.



1. INTRODUCTION

CuSbS_2 contains earth abundant elements and has promising optical properties, for example, a strong absorption coefficient.^{1–4} It has therefore been investigated as a photovoltaic absorber material for solar cell systems as a substitute for the CdTe and $\text{Cu}(\text{In}, \text{Ga})\text{Se}_2$ compounds.^{1–4} A band gap of 1 eV has previously been reported.⁵ CuSbS_2 has been fabricated using hybrid inks, thiol–amine mixtures, and electrochemically deposited metal stacks,^{6–8} yet very little is reported on bulk synthesis and characterization.

Mechanically induced reactions have been used in processing different materials for applications ranging from potential antibacterial materials, such as ZnO nanoparticles,⁹ to semiconductors, such as CoSb_3 for thermoelectric applications,^{10,11} as well as for organic materials synthesis.¹² The approach, also referred to as mechanical alloying or ball-milling in the literature, relies on mechanical agitation as a means to distribute energy for chemical processes.^{13–15} The process is sometimes considered a powder processing technique used to react elemental powders into homogeneous compounds, and often used as a complementary technique to solid-state, or liquid-phase, reaction of elements to form compounds. Ball-milling sometimes provides a more efficient bulk synthetic route than high-temperature synthetic approaches. The synthesis of CuSbS_2 is one such example; Marino et al.¹⁶ reported secondary phases from their high-temperature synthesis approach, whereas no impurities were observed in the X-ray diffraction (XRD) spectra of their ball-milled CuSbS_2 . In this report, we focus on the structural and transport properties of phase-pure ball-milled CuSbS_2 .

CuSbS_2 forms in an orthorhombic crystal structure (Figure 1a) with the $Pnma$ space group and contains several relatively short ionic bonds with four S atoms connecting each Cu atom

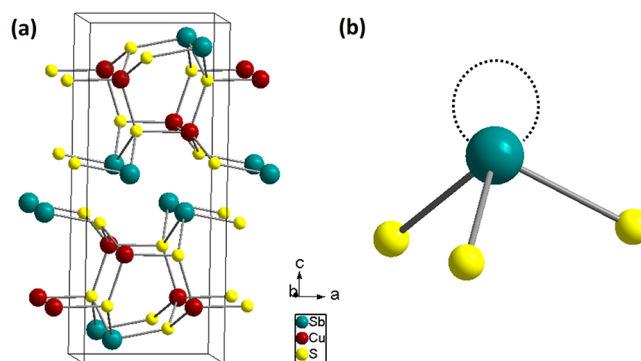


Figure 1. (a) CuSbS_2 crystal structure, and (b) Sb-S trigonal pyramid arrangement coordination environment where lone-pair electrons form.

in an almost tetrahedral arrangement.^{4,17} Three S atoms coordinate the Sb atoms in a trigonal pyramid arrangement (Figure 1b).^{4,17} As shown in Figure 1, the Sb 5s electrons form the “missing” corner of the distorted tetrahedron, thus allowing for lone-pair electron formation. As we will discuss below, this results in a very low thermal conductivity, κ , for this material. In addition to temperature dependent thermal conductivity and specific heat herein investigated, we report on the structural properties, electrical properties, optical band gap, and relative air stability at elevated temperatures, as well as the structural and transport properties of $\text{CuSbS}_{1.8}\text{Te}_{0.2}$ in order to compare with CuSbS_2 , as well as investigate the effect of alloying with Te.

Received: August 23, 2017

Published: October 30, 2017

2. EXPERIMENTAL SECTION

Phase-pure CuSbS_2 was synthesized by reaction of Cu powder (99.99%, Alfa Aesar), Sb chunk (99.95%, Alfa Aesar), and S powder (99.99%, Alfa Aesar) with a 1:1:2 compositional ratio by ball-milling.¹⁸ The powders were placed into a stainless steel container together with stainless steel balls in a powder mass ratio of 40:1. The container was then sealed under high purity Ar and loaded into a planetary ball mill. The synthesis time and ball mill speed were 6 h and 425 rpm, respectively. Densification was performed via hot pressing using custom tooling with a graphite die and molybdenum alloy punches at 603 K and 150 MPa for 3 h under continuous high purity N_2 flow. The resulting density measured by the Archimedes method, after hot pressing, was 4.52 g/cm^3 , with a packing density of 68%.¹⁹ $\text{CuSbS}_{1.8}\text{Te}_{0.2}$ was synthesized under identical conditions as CuSbS_2 , with nominal composition $\text{CuSbS}_{1.7}\text{Te}_{0.3}$ by the addition of Te powder (99.99%, Alfa Aesar). After hot pressing, we observed impurity phases, based on the XRD data. The densification of the Te-alloyed specimen was therefore best accomplished employing spark plasma sintering (SPS) as this technique allows for densification at lower temperatures and a significantly shorter holding time compared with that of hot pressing, thus reducing the formation of the impurity phases. SPS densification was done at 443 K and 400 MPa for 30 min under vacuum. The resulting density was 4.75 g/cm^3 , with a packing density of 72%.

Analysis of the specimens' homogeneity and stoichiometry was by Rietveld refinement of powder XRD data collected using a Bruker D8 Focus Diffractometer in Bragg–Brentano geometry with Cu $K\alpha$ radiation and a graphite monochromator, and Energy Dispersive Spectroscopy (EDS) using an Oxford INCA X-Sight 7852 equipped Scanning Electron Microscope (SEM, JEOL, JSM-6390LV). A TA Instruments Q600 was used to perform Differential Thermal Analysis (DTA) and Thermal Gravimetric Analysis (TGA) in order to determine the decomposition temperature. A separate piece of polycrystalline CuSbS_2 was used for air stability testing. UV–vis spectroscopy was measured on a finely ground powdered specimen, which was secured between two quartz slides, by a Jasco V-670 double beam spectrometer. A commercial Quantum Design Physical Property Measurement System performed heat capacity measurements from 2 to 393 K. The uncertainty (2σ) of the measurement is between 5.1% and 5.7% for the entire measured temperature range.

The densified pellets were cut, using a wire saw for transport measurements. A $2 \times 2 \times 11 \text{ mm}^3$ parallelepiped was used for four-probe high-temperature Seebeck coefficient, S , and electrical resistivity, ρ , measurements on a ULVAC ZEM-3 system under -0.05 MPa static He, with experimental uncertainty between 5% and 8%.²⁰ A 12.7 mm diameter and 1 mm thick disk was used for high-temperature laser flash thermal diffusivity measurements on a NETZSCH LFA475 system under flowing Ar, with an experimental uncertainty of 5%.

3. RESULTS AND DISCUSSION

Figure 2 shows the Rietveld refinement profiles of powder XRD data after densification that illustrates the observed data, the calculated data, and the difference between them. Table 1 shows the details of the refinement results and data collection, and Table 2 shows the atomic coordinates and displacement parameters. Table 3 shows the interatomic bond distances and bond angles for both specimens. The CuSbS_2 XRD data in Figure 2 show sharp line widths, whereas those from Marino et al.¹⁶ are very broad, an indication of potential defects or lattice strain. The compositions obtained from our EDS analyses are consistent with those obtained by our refinements. The crystal structures were refined with space group $Pnma$ (#62). The initial atomic positions and displacement parameters for the refinement were chosen based on mineral data of CuSbS_2 .¹⁷ Our analyses indicate that the composition is very close to nominal composition, with only the S sites having vacancies that are split evenly across both S sites. The Te containing

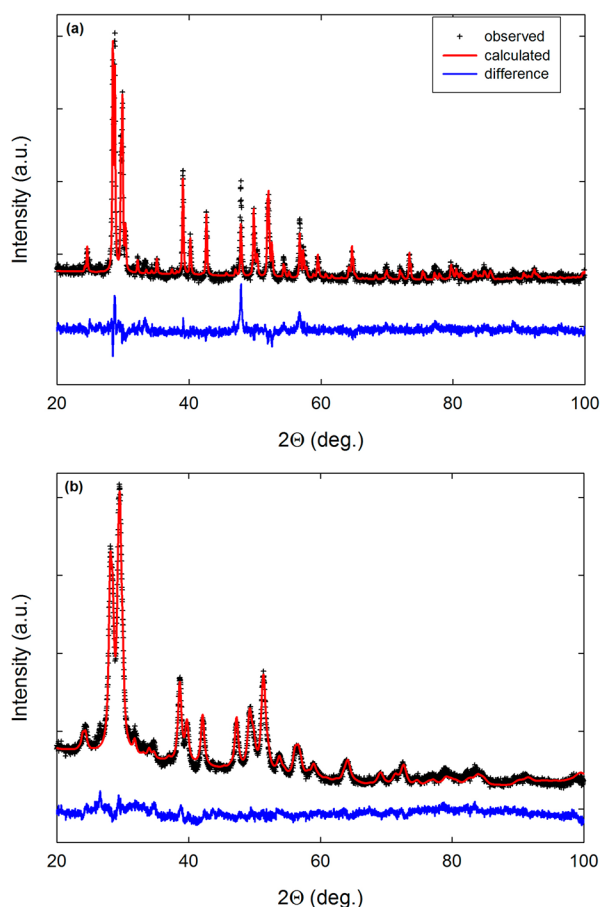


Figure 2. Powder XRD data for (a) CuSbS_2 and (b) $\text{CuSbS}_{1.8}\text{Te}_{0.2}$ including profile fit, profile difference, and profile residuals for Rietveld refinement. The higher background for $\text{CuSbS}_{1.8}\text{Te}_{0.2}$ is due to the specimen holder.

Table 1. Rietveld Refinement Parameters for the Two Compositions Prepared for This Report

nominal composition	CuSbS_2	$\text{CuSbS}_{1.7}\text{Te}_{0.3}$
composition	$\text{CuSbS}_{1.88}$	$\text{Cu}_{0.91}\text{Sb}_{0.96}\text{S}_{1.75}\text{Te}_{0.19}$
space group	$Pnma$ (#62)	$Pnma$ (#62)
a (Å)	6.0156(0)	6.0262(6)
b (Å)	3.7986(3)	3.8034(4)
c (Å)	14.4908(7)	14.4638(2)
V (Å ³)	331.1(3)	331.5(1)
radiation	graphite monochromated Cu $K\alpha$ (1.54056 Å)	
D_{calc} (g/cm^3)	4.92	5.38
2θ range (deg)	20–100	20–100
step width (deg)	0.025	0.025
wR_p , R_p	0.0617, 0.0458	0.0246, 0.0195
reduced χ^2	2.96	4.40

specimen has vacancies on the Cu and Sb sites. The S content is very close to that of the nominal composition for CuSbS_2 . The Te content is lower than the starting, nominal composition and is not evenly distributed over the S sites, with 4% and 15% occupancy of the S1 and S2 sites, respectively. This uneven distribution may be due to the larger bond lengths for Cu–S2 and Sb–S2 with respect to Cu–S1 and Sb–S1, as shown in Table 3. An increase in unit cell volume is observed for the Te containing composition, presumably due to the larger Te radius. The atomic positions and displacement parameters

Table 2. Atomic Coordinates and Displacement Parameters

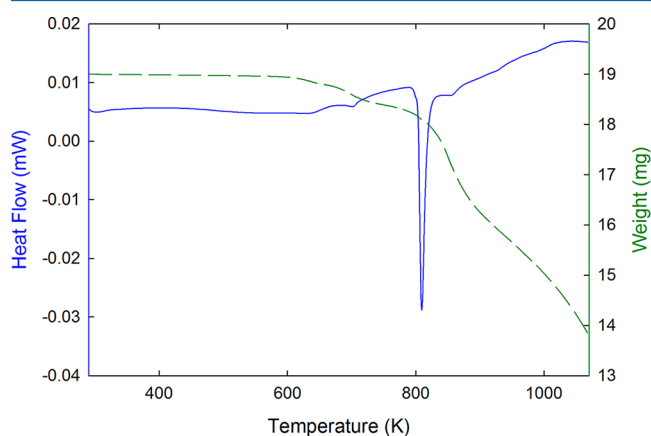
atoms	<i>x</i> (Å)	<i>y</i> (Å)	<i>z</i> (Å)	<i>U</i> _{iso} (Å ²)	occupancy
CuSbS ₂					
Cu	0.7392(3)	0.75	0.1754(3)	0.0252(3)	1.0
Sb	0.2267(1)	0.25	0.0610(5)	0.0269(1)	1.0
S1	0.6101(4)	0.25	0.1119(8)	0.0216(7)	0.96
S2	0.1173(9)	0.75	0.1658(7)	0.0209(3)	0.92
CuSbS _{1.8} Te _{0.2}					
Cu	0.7266(7)	0.75	0.1757(9)	0.0286(6)	0.91
Sb	0.2356(9)	0.25	0.0637(1)	0.0258(7)	0.96
S1	0.6271(7)	0.25	0.0963(7)	0.0242(1)	0.96
Te1	0.6015(7)	0.25	0.1123(5)	0.0194(5)	0.04
S2	0.0856(3)	0.75	0.1961(3)	0.0222(4)	0.79
Te2	0.1514(7)	0.75	0.1695(8)	0.0168(3)	0.15

shown in Table 2 are similar to those reported in the mineral data.¹⁷ The Te atoms have a smaller displacement parameter than S, attributed to both the presence of the lone-pair electrons associated with the Sb-S trigonal pyramid and the difference in size of the atoms. A reduction in the average Cu-S/-Te distance is observed (Table 3) for the Te containing composition. This reduction in Cu-S2 distances for the Te containing specimen would decrease the lattice parameter *a* due to the orientation of the 2.279(0) Å Cu-S2 bond. However, a decrease in the S2-Cu-S2 bond angle from 111.163(7)° for CuSbS₂ to 106.901(5)° (S2-Cu-S2), 93.708(3)° (S2-Cu-Te2), and 103.464(1)° (Te2-Cu-Te2) for CuSbS_{1.8}Te_{0.2} increases *a*. This combined with an increase in the S1-Sb-S2 bond angle results in an overall increase in the lattice parameter *a* for CuSbS_{1.8}Te_{0.2} with respect to CuSbS₂. The average Sb-S/-Te distances increase from 2.486(8) Å for CuSbS₂ to 2.673(2) Å for CuSbS_{1.8}Te_{0.2}. This increase in Sb-S/-Te bond lengths account for the larger *b* lattice parameter observed for CuSbS_{1.8}Te_{0.2}, as the Sb-S/-Te bonds mainly orient along *b*, although the increase in *b* is not as significant due to the decrease in the S2-Sb-S2 bond angles in CuSbS₂ compared to CuSbS_{1.8}Te_{0.2}. The reduction in *c* for the Te containing specimen can be attributed to the decrease in Cu-S2 bond length from 2.413(6) Å to 2.038(1) Å (Cu-S2) and 2.282(0) Å (Cu-Te2) that is oriented almost parallel to *c*.

Table 3. Interatomic Bond Distances and Bond Angles

		CuSbS _{1.88}	Cu _{0.91} Sb _{0.96} S _{1.75} Te _{0.19}		
Cu	-S1, -Te1	×2	2.248(5) Å	2.301(2) Å, 2.242(1) Å	
	-S2, -Te2		2.279(0) Å	2.183(1) Å, 2.561(5) Å	
	-S2, -Te2		2.413(6) Å	2.038(1) Å, 2.282(0) Å	
S1	-Cu	S1, Te1	115.277(5)°	111.457(7)°, 114.142(7)°	
S1	-Cu	S2, Te2	×2	108.655(4)°	108.992(6)°, 104.055(8)°
S1	-Cu	S2, Te2	×2	106.543(6)°	110.187(5)°, 115.947(4)°
S2	-Cu	S2, Te2		111.163(7)°	106.901(5)°, 93.708(3)°
Te1	-Cu	Te1			116.031(7)°
Te1	-Cu	S2, Te2	×2		112.850(6)°, 108.763(8)°
Te1	-Cu	S2, Te2	×2		103.402(4)°, 109.535(4)°
Te2	-Cu	Te2			103.464(2)°
Sb	-S1, -Te1		2.421(8) Å	2.406(0) Å, 2.314(3) Å	
	-S2, -Te2	×2	2.519(3) Å	2.846(6) Å, 2.493(8) Å	
S1	-Sb	S2, Te2	×2	93.720(8)°	100.333(7)°, 94.530(2)°
S2	-Sb	S2, Te2		97.857(9)°	83.835(8)°, 91.811(8)°
Te1	-Sb	S2, Te2	×2		95.630(4)°, 90.413(4)°
Te2	-Sb	Te2			99.383(8)°

Figure 3 shows DTA and TGA data for CuSbS₂. An endothermic decomposition is observed at 800 K. Powder XRD

**Figure 3.** DTA (solid) and TGA (dashed) data for CuSbS₂.

analysis after DTA/TGA measurements indicates that CuSbS₂ decomposed into Cu₁₂Sb₄S₁₃, implying that there is a loss of both Sb and S, which is in agreement with the fact that our TGA data shows a decrease in mass at elevated temperatures. This also indicates the possibility for another avenue for the synthesis of Cu₁₂Sb₄S₁₃, which has been reported to possess good thermoelectric properties.²¹ Air stability testing indicates that CuSbS₂ is stable in air up to 630 K even after being subjected to this temperature for several hours.

UV-vis spectroscopy of CuSbS₂ indicates an optical band gap, *E*_g, of 0.9 eV, in agreement with previously reported computational and experimental data.^{4,5} This data also suggests a direct optical band gap for CuSbS₂, from the rapid onset of absorption. The Te containing specimen also has a 0.9 eV band gap, although the onset of absorption is not as rapid, which may suggest an indirect band gap for this specimen. Figure 4a shows that the ρ values for these chalcogenides are relatively high and exhibit semiconductor behavior, decreasing with increasing temperature. CuSbS_{1.8}Te_{0.2} exhibits lower ρ values than that of the CuSbS₂ above 400 K. Figure 4b shows that the *S* values start increasing slightly with temperature at 400 K, and reach a

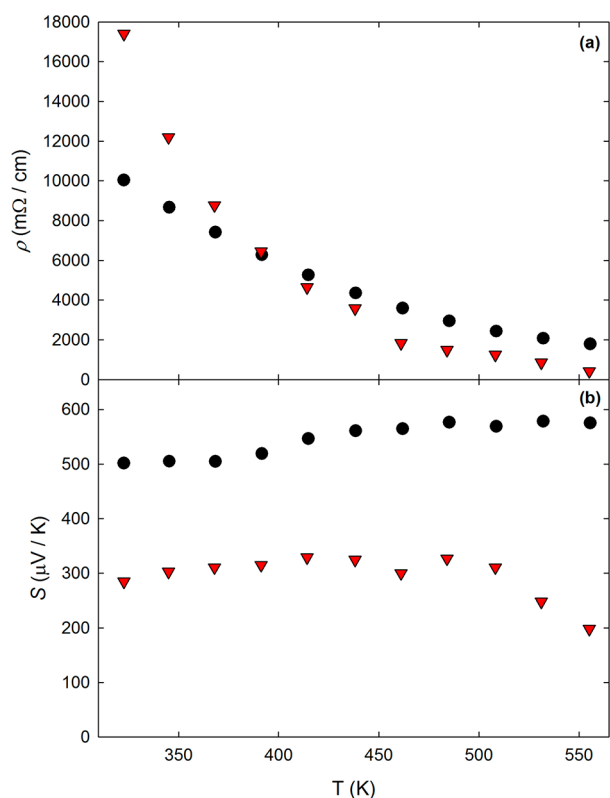


Figure 4. Temperature dependent (a) ρ and (b) S data for CuSbS_2 (circle) and $\text{CuSbS}_{1.8}\text{Te}_{0.2}$ (triangle).

peak value of 580 $\mu\text{V}/\text{K}$ at about 530 K for the CuSbS_2 specimen. The S values for $\text{CuSbS}_{1.8}\text{Te}_{0.2}$ are relatively temperature independent, $\sim 300 \mu\text{V}/\text{K}$, throughout the entire measured temperature range. These lower S values for the Te containing specimen are expected given the reduced ρ for this composition as compared to that of CuSbS_2 . The S values are positive for both specimens in the measured temperature range, implying hole majority carriers. These high S and ρ values can be expected given the relatively large E_g values.²²

Figure 5 shows isobaric heat capacity, C_p , measurements for 4.6 mg of CuSbS_2 in the temperature range of 2–390 K. The inset in Figure 5 shows low-temperature ($3 \text{ K} < T < 7 \text{ K}$) C_p/T

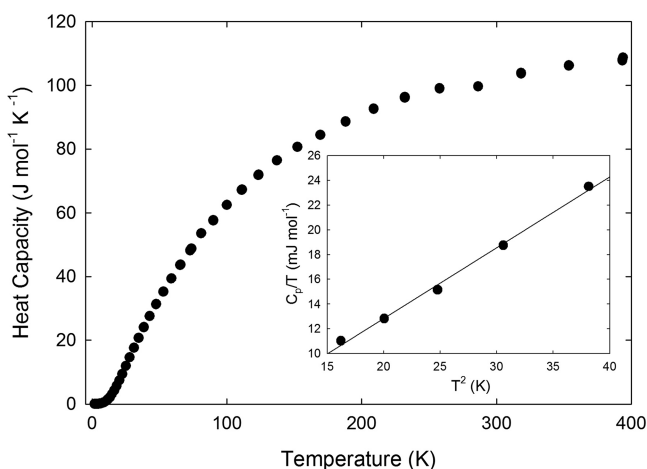


Figure 5. Temperature dependent C_p data for CuSbS_2 . The inset shows low-temperature data with a fit of the form $C_p/T = \beta T^2 + \gamma$.

versus T^2 data, where the straight line is a fit of the form $C_p/T = \beta T^2 + \gamma$. The slope of the linear fit (β) is the coefficient of the lattice contribution and the y -intercept (γ) is the Sommerfeld coefficient or electronic contribution to the specific heat.^{23,24} The values obtained by our simple fit are $\beta = 0.57 \text{ mJ mol}^{-1} \text{ K}^{-4}$ and $\gamma = 1.39 \text{ mJ mol}^{-1} \text{ K}^{-2}$. An estimate of the Debye temperature, Θ_D , can be obtained using the equation

$$\Theta_D = \left(\frac{12\pi^4 R n_a}{5\beta} \right)^{1/3} \quad (1)$$

where n_a is the number of atoms per unit cell, 16 for CuSbS_2 , and R is the molar gas constant. The resulting estimated value is $\Theta_D = 379 \text{ K}$, in good agreement with that reported for CuBiS_2 .²⁵ It can be assumed that the κ values shown in Figure 6

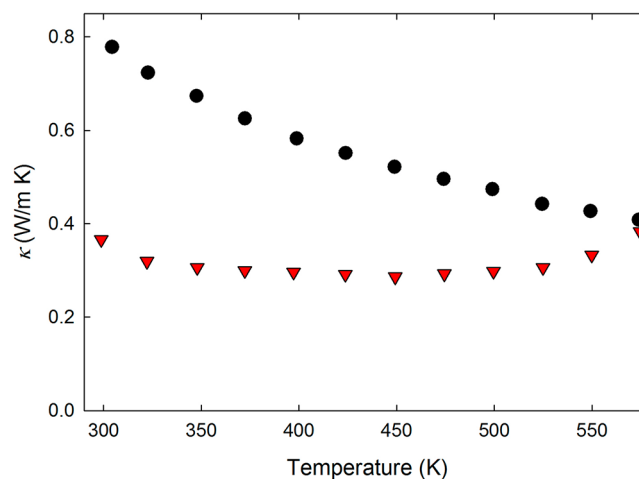


Figure 6. Temperature dependent κ data for CuSbS_2 (circle) and $\text{CuSbS}_{1.8}\text{Te}_{0.2}$ (triangle).

are dominated by the lattice contribution due to the specimen's high ρ values. Previous studies on certain chalcogenide compounds had indicated the presence of lone-pair electrons in ternary chalcogenide systems.^{4,26,27} The low κ values for CuSbS_2 are a result of the stereochemically active lone-pair electrons (Figure 1) that create anharmonicity in the lattice due to the electrostatic repulsion between the lone-pair electrons and the neighboring chalcogen ions. These κ values are lower than those reported for other chalcogenide materials that also exhibit lone-pair electron bonding.^{26–28} The κ values are further reduced by Te alloying, presumably due to the large difference in mass between S and Te, as well as potential further mass fluctuation scattering from vacancies (Table 2), resulting in lower κ values for $\text{CuSbS}_{1.8}\text{Te}_{0.2}$ over the entire measured temperature range.

4. CONCLUSION

Phase-pure synthesis of CuSbS_2 via ball-milling was achieved for the first time. This method requires much less synthesis time than the traditional direct reaction method. Rietveld refinement indicates high crystalline quality for CuSbS_2 . $\text{CuSbS}_{1.8}\text{Te}_{0.2}$ was similarly synthesized in order to compare to CuSbS_2 . The $\text{CuSbS}_{1.8}\text{Te}_{0.2}$ specimen shows a reduced ρ compared to that of CuSbS_2 , presumably due to the vacancies in the Te-alloyed specimen as compared with CuSbS_2 . Low κ values for both components is attributed to the anharmonicity caused by the stereochemically active s^2 lone-pair electrons,

while Te alloying further reduces κ . These specimens exhibit behavior useful for possible applications as thermal barrier materials.²⁹ Further alloying or composites with appropriate composite materials²⁷ may be avenues to improve the thermoelectric properties, and consequently enable these materials to be of interest for further research for thermoelectric applications.

AUTHOR INFORMATION

Corresponding Author

*E-mail: gnolas@usf.edu.

ORCID

George S. Nolas: 0000-0001-8741-1678

Notes

The authors declare no competing financial interest.

ACKNOWLEDGMENTS

This work was supported, in part, by the National Science Foundation Grant No. DMR-1400957. D.H. and K.W. also acknowledge support from the II-VI Foundation Block-Gift Program. H.W. would like to acknowledge the support of the assistant secretary for Energy Efficiency and Renewable Energy of the Department of Energy and the Propulsion Materials program under the Vehicle Technologies program. Oak Ridge National Laboratory is managed by UT-Battelle LLC under contract DE-AC05000OR22725. The authors thank Dr. Jeff Sharp of Marlow Industries for air stability testing.

REFERENCES

- (1) Yang, B.; Wang, L.; Zhou, Y.; Song, H.; Chen, S.; Zhong, J.; Lv, L.; Niu, D.; Tang, J.; Han, J. CuSbS₂ as a Promising Earth-Abundant Photovoltaic Absorber Material: A Combined Theoretical and Experimental Study. *Chem. Mater.* **2014**, *26*, 3135–3143.
- (2) Kumar, M.; Persson, C. CuSbS₂ and CuBiS₂ as potential absorber materials for thin-film solar cells. *J. Renewable Sustainable Energy* **2013**, *5*, 031616.
- (3) Liu, Z.; Huang, J.; Han, J.; Hong, T.; Zhang, J.; Liu, Z. CuSbS₂: a promising semiconductor photo-absorber material for quantum dot sensitized solar cells. *Phys. Chem. Chem. Phys.* **2016**, *18*, 16615–16620.
- (4) Dufton, J. T. R.; Walsh, A.; Panchmatia, P. J.; Peter, L. M.; Colombara, D.; Islam, M. S. Structural and electronic properties of CuSbS₂ and CuBiS₂: potential absorber materials for thin-film solar cells. *Phys. Chem. Chem. Phys.* **2012**, *14*, 7229–7233.
- (5) Zhou, J.; Bian, G. Q.; Zhu, Q. Y.; Zhang, Y.; Li, C. Y.; Dai, J. Solvothermal crystal growth of CuSbQ₂ (Q = S, Se) and the correlation between macroscopic morphology and microscopic structure. *J. Solid State Chem.* **2009**, *182*, 259–264.
- (6) Septina, W.; Ikeda, S.; Iga, Y.; Harada, T.; Matsumura, M. Thin film solar cell based on CuSbS₂ absorber fabricated from an electrochemically deposited metal stack. *Thin Solid Films* **2014**, *550*, 700–704.
- (7) McCarthy, C. L.; Cottingham, P.; Abuyen, K.; Schueller, E. C.; Culver, S. P.; Brutchey, R. L. Earth abundant CuSbS₂ thin films solution processed from thiol-amine mixtures. *J. Mater. Chem. C* **2016**, *4*, 6230–6233.
- (8) Banu, S.; Ahn, S. J.; Ahn, S. K.; Yoon, K.; Cho, A. Fabrication and characterization of cost-efficient CuSbS₂ thin film solar cells using hybrid inks. *Sol. Energy Mater. Sol. Cells* **2016**, *151*, 14–23.
- (9) Salah, N.; Habib, S. S.; Khan, Z. H.; et al. High-energy ball milling technique for ZnO nanoparticles as antibacterial material. *Int. J. Nanomed.* **2011**, *6*, 863–869.
- (10) Yang, J.; Chen, Y.; Peng, J.; Song, X.; Zhu, W.; Su, J.; Chen, R. Synthesis of CoSb₃ skutterudite by mechanical alloying. *J. Alloys Compd.* **2004**, *375*, 229–232.
- (11) Liu, K.; Jiuxing, Z.; Dong, X. The exploration for synthesizing CoSb₃ powder by mechanical alloying. *J. Mater. Process. Technol.* **2007**, *184*, 257–260.
- (12) Stolle, A.; Szuppa, T.; Leonhardt, S. E. S.; Ondruschka, B. Ball milling in organic synthesis: solutions and challenges. *Chem. Soc. Rev.* **2011**, *40*, 2317–2329.
- (13) McCormick, P. G. Application of Mechanical Alloying to Chemical Refining. *Mater. Trans., JIM* **1995**, *36*, 161–169.
- (14) Suryanarayana, C. Mechanical alloying and milling. *Prog. Mater. Sci.* **2001**, *46*, 1–184.
- (15) Takacs, L. Self-sustaining reactions induced by ball milling: An overview. *Int. J. Self-Propag. High-Temp. Synth.* **2009**, *18*, 276–282.
- (16) Marino, C.; Block, T.; Pöttgen, R.; Vilevieille, C. CuSbS₂ as a negative electrode material for sodium ion batteries. *J. Power Sources* **2017**, *342*, 616–622.
- (17) Kyono, A.; Kimata, M. Crystal structures of chalcostibite (CuSbS₂) and emplectite (CuBiS₂): Structural relationship of stereochemical activity between chalcostibite and emplectite. *Am. Mineral.* **2005**, *90*, 162–165.
- (18) Certain commercial equipment, instrumentation, or materials are identified in this document. Such identification does not imply recommendation or endorsement by the National Institute of Standards and Technology, nor does it imply that the products identified are the best available for the purpose.
- (19) Kittel, C. *Introduction to Solid State Physics*; John Wiley & Sons: New York, 1976.
- (20) Martin, J.; Tritt, T. M.; Uher, C. High temperature Seebeck coefficient metrology. *J. Appl. Phys.* **2010**, *108*, 121101.
- (21) Lu, X.; Morelli, D. T.; Wang, Y.; Lai, W.; Xia, Y.; Ozolins, V. Phase Stability, Crystal Structure, and Thermoelectric Properties of Cu₁₂Sb₄S_{13-x}Se_x Solid Solutions. *Chem. Mater.* **2016**, *28*, 1781–1786.
- (22) Goldsmid, H. J.; Sharp, J. W. Estimation of the Thermal Band Gap of a Semiconductor from Seebeck Measurements. *J. Electron. Mater.* **1999**, *28*, 869–872.
- (23) Aydemir, U.; Candolfi, C.; Bornmann, H.; Baitinger, M.; Ormeci, A.; Carrillo-Cabrera, W.; Chubilleau, C.; Lenoir, B.; Dauscher, A.; Oeschler, N.; Steglich, F.; Grin, Y. Crystal structure and transport properties of Ba₈Ge₄₃. *Dalton Trans.* **2010**, *39*, 1078–1088.
- (24) Singh, Y.; Lee, Y.; Nandi, S.; Kreyssig, A.; Ellern, A.; Das, S.; Nath, R.; Harmon, B. N.; Goldman, A. I.; Johnston, D. C. Single-crystal growth and physical properties of the layered arsenide BaRh₂As₂. *Phys. Rev. B: Condens. Matter Mater. Phys.* **2008**, *78*, 104512.
- (25) Zhang, Z. R.; Zeng, D. P.; Xie, L. H.; Deng, X. P.; Song, K. H. First-Principles Study of the Elastic and Thermodynamic Properties of CuBiS₂ Photovoltaic Absorber Material. *Chalcogenide Lett.* **2014**, *11*, 661–670.
- (26) Skoug, E. J.; Morelli, D. T. Role of Lone-Pair Electrons in Producing Minimum Thermal Conductivity in Nitrogen-Group Chalcogenide Compounds. *Phys. Rev. Lett.* **2011**, *107*, 235901–235905.
- (27) Zhang, D.; Yang, J.; Jiang, Q.; Fu, L.; Xiao, Y.; Luo, Y.; Zhou, Z. Ternary CuSbSe₂ chalcostibite: facile synthesis, electronic-structure and thermoelectric performance enhancement. *J. Mater. Chem. A* **2016**, *4*, 4188.
- (28) Dong, Y.; Khabibullin, A. R.; Wei, K.; Salvador, J. R.; Nolas, G. S.; Woods, L. M. Bournonite PbCuSbS₃: Stereochemically Active Lone-Pair Electrons that Induce Low Thermal Conductivity. *ChemPhysChem* **2015**, *16*, 3264–3270.
- (29) Wan, C. L.; Pan, W.; Xu, Q.; Qin, Y. X.; Wang, J. D.; Qu, Z. X.; Fang, M. H. Effect of point defects on the thermal transport properties of (La_xGd_{1-x})₂Zr₂O₇: Experiment and theoretical model. *Phys. Rev. B: Condens. Matter Mater. Phys.* **2006**, *74*, 144109.